Regularizing firing patterns of rat subthalamic neurons ameliorates parkinsonian motor deficits

Qian-Xing Zhuang,[1] Guang-Ying Li,[1] Bin Li,[1] Chang-Zheng Zhang,[1] Xiao-Yang Zhang,[1] Kang Xi,[1] Hong-Zhao Li,[1] Jian-Jun Wang,[1,2] and Jing-Ning Zhu[1,2]

[1]State Key Laboratory of Pharmaceutical Biotechnology and Department of Physiology, School of Life Sciences, Nanjing University, 163 Xianlin Avenue, Nanjing 210023, China
[2]Institute for Brain Sciences, Nanjing University, 163 Xianlin Avenue, Nanjing 210023, China

Authorship note: Q.-X.Z., G.-Y.L. and B.L. contributed equally to this work.

Conflict of interests: The authors have declared that no conflict of interest exists.

Address correspondence to: Jing-Ning Zhu, State Key Laboratory of Pharmaceutical Biotechnology and Department of Physiology, School of Life Sciences, Nanjing University, 163 Xianlin Avenue, Nanjing 210023, China. Phone: 86.25.89682714; Fax: 86.25.89682705; E-mail: jnzhu@nju.edu.cn. Or to: Jian-Jun Wang, State Key Laboratory of Pharmaceutical Biotechnology and Department of Physiology, School of Life Sciences, Nanjing University, 163 Xianlin Avenue, Nanjing 210023, China. Phone: 86.25.89682714; Fax: 86.25.89682705; E-mail: jjwang@nju.edu.cn.

Abstract

The subthalamic nucleus (STN) is an effective therapeutic target for deep brain stimulation (DBS) for Parkinson's disease (PD) and histamine level is elevated in the basal ganglia in PD patients. However, the endogenous histaminergic modulation on STN neuronal activities and the neuronal mechanism underlying STN-DBS are unknown. Here we report that STN neuronal firing patterns are more crucial than firing rates for motor control. Histamine excited STN neurons, but paradoxically ameliorated parkinsonian motor deficits, which we attributed to regularizing firing patterns of STN neurons via HCN2 channel coupled to H2 receptor. Intriguingly, DBS increased histamine release in the STN and regularized STN neuronal firing patterns under parkinsonian conditions. HCN2 contributed to the DBS-induced regularization of neuronal firing patterns, suppression of excessive beta oscillations, and alleviation of motor deficits in PD. The results reveal an indispensable role for regularizing STN neuronal firing patterns in amelioration of parkinsonian motor dysfunction and a functional compensation for histamine in parkinsonian basal ganglia circuitry. The findings provide insights into mechanisms of STN-DBS as well as potential therapeutic targets and STN-DBS strategies for PD.

Introduction

The subthalamic nucleus (STN), the only excitatory structure in the basal ganglia, holds a key position in the basal ganglia circuitry and is an optimal clinical target for deep brain stimulation (DBS) (1, 2) for treatment of motor symptoms in Parkinson's disease (PD). The STN not only constitutes the classic indirect pathway (3-5) and the hyperdirect cortico-STN-pallidal pathway (6-8), but also serves as a central pacemaker for the basal ganglia circuitry (9). Although the hypothesis of activating (cortical) afferents/passing fibers to the STN has been proposed and prevalently accepted (10, 11), the precise therapeutic mechanisms of STN-DBS remain undefined, which constrains the optimization and development of DBS strategies. Notably, in PD patients (12-16) and nonhuman primate (3, 17, 18) and rodent (11, 19-21) models of PD, abnormal irregular neuronal firing rates, firing patterns, and network oscillations are recorded in the STN, indicating a close relationship between the abnormal STN neuronal activities and parkinsonian motor deficits. Yet little is known about the intrinsic properties and endogenous modulators responsible for modulation of STN neuronal activities. Uncovering these intrinsic and endogenous substrates will help understand the pathophysiology of PD and the neuronal mechanism underlying STN-DBS.

Intriguingly, a significant increase in histamine levels and a functional alternation in the histaminergic system in the basal ganglia are revealed in PD patients (22-24). Central histamine, restrictedly synthesized in the tuberomammillary nucleus (TMN) of the hypothalamus, has been well known to be a general modulator for whole brain functions (25, 26), including not only sleep/wakefulness (27, 28) but also motor control (29, 30). Nevertheless, role of histamine and

central histaminergic system in the basal ganglia motor function and PD pathophysiology is controversial. Since its level is elevated in PD, histamine has been implicated in either deterioration of PD, or sleep disorders and nonmotor dysfunctions in PD, but less associated with motor symptoms (31, 32). Here we report, however, that endogenous histamine/histaminergic system is essential for regularizing STN neuronal firing patterns, which are more crucial than firing rates for maintenance of normal basal ganglia motor function. The hyperpolarization-activated cyclic nucleotide-gated (HCN) channel 2 contributes to regularization of firing patterns of STN neurons by not only histaminergic inputs but also high-frequency DBS, both of which ameliorate parkinsonian motor deficits. Regularizing firing patterns of STN neurons in PD may account for why STN-DBS restores motor function in PD.

Results

Histamine level is gradually increased in STN of PD rats and histamine ameliorates PD motor impairment.

We first detected histamine levels in bilateral STNs (Figure 1A) in the 6-hydroxydopamine (6-OHDA)-lesioned rat model of hemiparkinsonian (Supplemental Figure 1A). The histamine level in the ipsilesional STN (Figure 1B) was gradually increased with the damage of dopaminergic neurons (Supplemental Figure 1B) and the decrease of dopamine levels (Supplemental Figure 1C) in the substantia nigra, whereas that in the contralesional STN maintains normal. Mapping the histaminergic

projections in the STN by anterograde tracings showed that the histamine-immunoreactive fibers originating from the histaminergic neurons in the TMN (Figure 1C, left panel) were scattered throughout the STN (Figure 1C, right panel). These histaminergic fibers possessed prominent varicosities and passed around glutamatergic neurons in the STN (Figure 1C, right panel), suggesting a neural modulation on STN neurons may occur by histamine released from the histaminergic terminals. Concurrent with the increase in histamine level, the histaminergic fiber density was also increased in the ipsilesional rather than contralesional STN (Supplemental Figure 1D) in PD rats.

Figure 1 near here

Histamine is known as a homogeneous excitatory modulator on various brain regions (25, 26). According to the classic model of basal ganglia (5, 33), increase in STN neuronal firing rates leads to enhancing the activity of indirect pathway to inhibit movement. Thus, if histamine excites STN neurons, the seemingly logical conclusion is that the excitatory modulation of histamine on STN results in deteriorating motor deficits in PD. However, surprisingly, unlike high K^+, histamine locally microinjected into the ipsilesional STN decreased the apomorphine-induced turnings in PD rats (Figure 1D), i.e., ameliorating the parkinsonian motor impairment.

Histamine rather than high K^+ regularizes firing patterns of STN neurons in PD rats both in vivo and in vitro.

Thus, we were curious about the mechanism underlying the amelioration effect of histamine on parkinsonian motor dysfunction. We examined the effect of histamine on single-unit firing in STN by spike sorting and analysis of multichannel recordings in vivo. As expected, both histamine and high K^+ induced a significant increase in firing rates of STN neurons in normal and PD rats (Figure 2, A, D and G). But, intriguingly, by analyzing unit firing autocorrelograms (Figure 2B), inter-spike interval (ISI) histograms (Figure 2C), and coefficient of variation (CV) of ISIs (Figure 2H), we found that histamine, instead of high K^+, increased periodicity of STN neuronal firing, narrowed ISI distributions and decreased the CV of ISIs in normal rats. These results suggest that histamine may regularize firing patterns of STN neurons. Comparing with normal rats, STN neurons in PD rats exhibited an increase in firing rates (Figure 2G) and a concomitantly irregular firing pattern with a loss of periodicity of discharges (Figure 2B, left panel, and 2E, left panel), altered ISI distributions (Figure 2, C and F), an increased CV of ISIs (Figure 2H), as well as an increased number of bursts and a shortened inter-burst intervals (Figure 2I), which are in accord with previous observations in both PD patients and animal models (3, 34-36). Notably, histamine significantly restored STN neuronal firing patterns in parkinsonian conditions both in vivo (Figure 2, E, F, H and I) and in vitro (Supplemental Figure 2), but high K^+ had no such effect. Therefore, we suggest that regularization of firing patterns of STN neurons may account for why histamine ameliorates motor dysfunction in PD.

Figure 2 near here

H2 receptor and its coupled HCN channel mediate the histamine-induced regularization of STN neuronal firing patterns and amelioration of PD motor deficits.

We assessed receptor and ionic mechanisms underlying the effect of histamine on STN neurons by whole-cell patch clamp recordings in vitro (Figure 3A). Histamine directly induced an inward current on STN neurons in a concentration dependent manner (Supplemental Figure 3, A and B) and did not influence miniature EPSCs and IPSCs (Supplemental Figure 3, C and D), suggesting a direct postsynaptic effect of histamine. This effect was mediated by postsynaptic histamine H2 rather than H1 and H4 receptors (Supplemental Figure 3, E and F). Single-cell qPCR and immunofluorescence results confirmed that only H2 receptor was expressed and localized in STN neurons (Supplemental Figure 4). Furthermore, the membrane conductance of STN neurons exhibited a significant feature of hyperpolarization activation (Figure 3B) and the hyperpolarization-activated current was reversed at -31 mV (Supplemental Figure 5A), which is near the reversal potential of HCN channel (37). Histamine increased not only the hyperpolarization-activated conductance (Figure 3B) but also the depolarizing sag (Figure 3C, left panel), which is triggered by the activation of HCN channel. ZD7288 (50 μM), a selective blocker for HCN channel, abolished the depolarizing sag (Figure 3C, middle and right panels) and the histamine-induced hyperpolarization-activated inward current (Supplemental Figure 5B), which was also blocked by ranitidine, a selective antagonist for H2 receptor (Figure 3D). Thus, HCN channel coupled to H2 receptor mediates the effect of histamine on STN neurons. More importantly, both ranitidine and a low concentration of ZD7288 (1 μM) effectively blocked the histamine-induced increase in the regularity of STN neuronal firing patterns in normal rats (Figure 3,

E-G), indicating that HCN channel is responsible for regularizing firing patterns of STN neurons by histamine.

Figure 3 near here

To further examine whether H2 receptor and its coupled HCN channel mediate the histamine-induced amelioration of motor deficits in PD, we evaluated motor performances by means of pharmacological manipulation on histaminergic modulation on STN. Electrophysiological and histological methods were employed to identify microinjection sites and effective spread in the STN (Supplemental Figure 6). Microinjected histamine significantly increased the firing rate and decreased the CV of ISIs on STN neurons close to the injection sites, whereas ranitidine decreased the firing rate and increased the CV of ISIs by antagonizing H2 receptor to block endogenous histaminergic inputs (Supplemental Figure 6B). Neither histamine nor ranitidine influenced neurons in the border between STN and zona incerta (Supplemental Figure 6, A and C), indicating a manipulation confined within the STN. As shown in Figure 4, blocking histaminergic inputs by ranitidine in STN significantly increased the apomorphine-induced turnings in PD rats, whereas dimaprit, a selective agonist for H2 receptor, mimicked the histamine-induced decrease in turnings (Figure 4A). However, microinjection of antagonists or agonists for H1, H3 or H4 receptor into STN had no effect on the turning behavior of PD rats (Supplemental Figure 7), which is consistent with our above-mentioned electrophysiological and single-cell qPCR results. Blocking HCN channel by ZD7288 not only increased the turnings of PD rats but also abolished the histamine-induced decrease in turnings (Figure 4A). In addition, we assessed slowness of motor initiation and execution of PD

rats by adhesive removal test (Figure 4B) and gait disturbance by footprint test (Figure 4C). We found that microinjection of histamine into STN significantly shortened the prolonged time for removing a rectangular adhesive strip from contralesional forelimb (Figure 4B) and enlarged bilateral stride lengths instead of stride width (Figure 4C). On the other hand, the effects of histamine were mimicked by dimaprit and attenuated by ranitidine and ZD7288 (Figure 4, B and C). These results suggest that histaminergic modulation on STN may remedy bradykinesia and gait disturbance in PD via H2 receptor and HCN channel. Therefore, H2 receptor and its coupled HCN channel contribute to the histamine-induced amelioration of parkinsonian motor deficits.

Figure 4 near here

Given the fact that histamine regularizes firing patterns of STN neurons and restores PD motor deficits, we speculate that a gradual rise of histamine level in STN in PD progression may be a compensatory result for abnormal irregular firing patterns of STN neurons, and the enhanced histaminergic modulation may help to improve normal motor function of basal ganglia. As expected, in normal rats, bilateral microinjection of histamine into STN promoted motor performances in accelerating rota-rod and balance beam, and blockage of endogenous histaminergic inputs by blocking H2 receptor or HCN channel attenuated motor performances (Supplemental Figure 8). Therefore, histaminergic modulation may serve as an indispensable biasing force for the basal ganglia circuity, which not only maintains normal motor functions but also alleviates parkinsonian motor dysfunctions.

HCN2 channel is responsible for the amelioration of motor deficits in PD rats by histamine.

In mammals, four HCN channel subtypes have been identified (38-40) and all of them were expressed and localized in the STN (Supplemental Figure 9). Interestingly, the activation curve for HCN conductance in STN neurons showed that the channel was activated slowly at hyperpolarized potentials more negative than -70 mV (Figure 3B), and the membrane potential for half-maximal activation ($V_{1/2}$ = 95.8 ±0.86 mV) was closer to that of the cloned HCN2 (40, 41) and was significantly shifted by histamine towards the depolarizing direction (Figure 3B). The results indicate an activation of HCN2 channel by histamine on STN neurons. To further assess the contribution of each HCN channel subtype to the histamine-induced motor improvements in PD rats, we generated lentiviral vectors to separately downregulate the expression of each subtype of HCN channel in STN (Figure 5, A-D, Supplemental Figure 10 and Supplemental Table 1). Properties of HCN channel in STN neurons did not change in PD (Supplemental Figure 11, A, B, D, and E), but HCN2 downregulation decreased the depolarizing sag and HCN current in STN neurons (Supplemental Figure 11, C-E). Accordingly, downregulation of HCN2 significantly increased the apomorphine-induced turnings (Figure 5F), prolonged contralesional rather than ipsilesional adhesive removal time (Figure 5G, and Supplemental Figure 12A), and shortened stride length instead of stride width (Figure 5H, and Supplemental Figure 12B) in PD rats, whereas downregulation of HCN1, HCN3, or HCN4 had no effect on these motor deficits (Figure 5, F-H). Moreover, the histamine-induced motor improvements in PD rats were blocked by downregulation of HCN2 rather than HCN1, HCN3, or HCN4 (Figure 5, F-H). On the other hand, overexpression of HCN2 channel in STN (Figure 5E) not only restored motor deficits of

PD rats, but also promoted the histamine-induced improvements (Figure 5, F-H, and Supplemental Figure 12). In normal rats, downregulation of HCN2 rather than HCN1, HCN3, or HCN4 remarkably attenuated motor performances on an accelerating rota-rod and a balance beam and the histamine-induced motor improvements (Supplemental Figure 13, A and B), whereas overexpression of HCN2 significantly improved motor performances and the histamine-induced improvements (Supplemental Figure 13, C and D). Since HCN2 channel is co-localized with H2 receptor on STN neurons (Supplemental Figure 14) and selectively expressed in the glutamatergic instead of GABAergic neurons in the STN (Supplemental Figure 15), we suggest that HCN2 rather than HCN1, 3, and 4 channel may be coupled to H2 receptor and contribute to the histaminergic modulation on STN glutamatergic projection neurons and the consequent amelioration of parkinsonian motor dysfunction and improvement of normal motor function.

Figure 5 near here

HCN2 channel contributes to the DBS-induced regularization of STN neuronal firing patterns, suppression of beta oscillations, and alleviation of motor deficits in PD rats.

We further determined the role of HCN2 channel in regularization of firing patterns of STN neurons under parkinsonian condition. As shown in Figure 6, A-F, firing patterns of STN neurons in PD rats with overexpression of HCN2 in STN were more regular than those in untreated PD rats. In contrast, downregulation of HCN2 made STN neuronal firing patterns more irregular (Figure 6, A-F).

It is noteworthy that overexpression of HCN2 in STN neurons ameliorated motor deficits, whereas downregulation of HCN2 deteriorated motor dysfunctions (Figure 5, F-H). These results strongly indicate that HCN2 channel may play an important role in regularizing firing patterns of STN neurons, which is critical for basal ganglia motor functions. Considering STN is an optimal target for clinical DBS treatment for PD and abnormal irregular firing patterns are recorded in the STN neurons in PD patients (34, 42, 43), we wonder whether DBS influence the regularity of STN neuronal firing patterns. Intriguingly, we found that high-frequency stimulation of STN remarkably regularized neuronal firing patterns of PD rats and firing patterns became irregular again when DBS ceased (Figure 6, G-L), suggesting that regularization of firing patterns of STN neurons may account for the therapeutic effect of DBS on motor dysfunctions in PD.

Figure 6 near here

Furthermore, we investigated the role of HCN2 channel in the STN-DBS-induced amelioration of motor dysfunctions and regularization of STN neuronal firing patterns in free-moving PD rats. As shown in Figure 7A, high-frequency DBS of STN significantly increased total movement distance of PD rats in an open field as previously reported (11), indicating STN-DBS effectively ameliorates parkinsonian locomotor impairment. In contrast, PD rats with downregulation of HCN2 did not exhibit improvements of locomotion during STN-DBS (Figure 7A), suggesting HCN2 channel is critical for the DBS-induced remedy of locomotor deficit. Notably, the STN-DBS-induced motor improvement in free-moving PD rats was accompanied by an increase in histamine release in the

STN (Figure 7B) and a regularization of firing patterns of numerous individual STN neurons (Figure 7, C-H), as well as a suppression of exaggerated oscillatory network synchronization at the beta band (15-25 Hz) (Figure 7, I and J), which is prevalent in STN of animal models and patients with PD (44-46). Furthermore, downregulation of HCN2 abolished the STN-DBS-induced regularization of neuronal firing patterns in free-moving PD rats (Figure 7, C-H) and alleviation of excessive beta oscillations (Figure 7, I and J). All these results strongly suggest that HCN2 channel may contribute to the STN-DBS-induced regularization of STN neuronal firing patterns and the consequent amelioration of motor deficits in PD.

Figure 7 near here

Discussion

Both firing rates and firing patterns of STN neurons are implicated in pathophysiology of PD (3, 17, 21, 36, 47, 48). Here, we demonstrate that firing patterns of STN neurons are more critical for basal ganglia motor function than firing rates. Increasing the firing rates of STN neurons, for instance by high K^+, deteriorates motor deficits of a 6-OHDA-lesioned rat model of PD (Figure 1D), which is in agreement with the classic direct/indirect pathway model of basal ganglia (3, 5) and the alleviation of parkinsonian motor dysfunction by lesioning STN (17) or reducing STN neuronal activities (49, 50). On the contrary, histamine, which also exerts an excitatory effect on STN neuronal activity (Figure 2, A, D and G), paradoxically ameliorates the apomorphine-induced turning,

bradykinesia, and gait disturbance of PD rats (Figure 4). Considering that high K^+ does not influence firing patterns of STN neurons but histamine significantly regularizes them (Figure 2), we propose that the improvement of abnormal irregular STN neuronal firing patterns as a fundamental contributor to the histamine-induced amelioration of parkinsonian motor deficits. Therefore, we suggest that the histaminergic modulation is crucial for maintenance of normal STN neuronal firing patterns and basal ganglia motor functions. The increase in histamine level and histaminergic afferent density in PD progression may play a compensatory role for amelioration of abnormal STN neuronal firing patterns and parkinsonian motor deficits. In fact, several histaminergic agents have been empirically used in clinic for treatment of not only parkinsonian non-motor symptoms but also motor dysfunctions as adjuvant drugs (51, 52). Thus, restoration of normal firing patterns of STN neurons by targeting histaminergic system and related ion channels may be an effective strategy for treatment of PD motor symptoms.

HCN channel is well known to hold a key position in accelerating neuronal depolarization to generate pacemaking rhythmic activity and control firing pattern (19, 37). However, previous studies indicated that HCN channel played minimal roles in the autonomous single-spiking firing of STN neurons (53, 54). In contrast, we find that HCN channel coupled to H2 receptor substantially mediates the histamine-induced regularization of firing patterns of STN neurons and improvement of motor deficits in PD rats (Figures 3-5), strongly suggesting a key position of HCN channel in STN neuronal firing patterns. Although our data and previous study (53) show that four subtypes of HCN channels (HCN1-4) have all been expressed in the STN, only HCN2 channel contributes to the amelioration of PD motor deficits by histamine/histaminergic afferent inputs. Furthermore, it is

important to indicate that upregulation of HCN2 increases the regularity of STN neuronal firing patterns in PD rats, while downregulation makes the irregular firing patterns much worse (Figures 6, A-F and 7, C-J) and consequently abolishes both the histamine-induced (Figure 5, F-H) and the DBS-evoked (Figure 7A) ameliorations of parkinsonian motor dysfunction. Given the facts that HCN2 promotes single-spike activity rather than burst firing (19, 55), and suppression of burst-generating capacity in STN remedies bradykinesia (21, 36), we suggest that HCN2 channel may hold an essential position in normal rhythm patterns of STN neuronal firing activity and subsequent motor function of basal ganglia.

Interpretations of therapeutic mechanisms underlying the DBS in STN for treatment on motor dysfunctions in PD remain controversial, with prevalent view shifting from inhibiting excessive STN activity (3, 17) to activating cortical afferents/passing fibers to the STN (10, 11). But, electrical stimulation of cortex for alleviation of PD motor symptoms in humans have proven disappointing (2). Although many studies have suggested a close correlation between the abnormal beta network oscillations and PD pathophysiology as well as STN-DBS (13-16, 18, 20, 44-46, 56), there is little direct evidence to establish the exact role of STN neuronal firing patterns in DBS therapeutic effect. Our data, in implicating DBS directly increases the endogenous histamine release, and subsequently regularizes STN neuronal firing patterns and suppresses excessive beta network oscillations to ameliorate parkinsonian motor impairments via HCN2 channel (Figures 6, G-L and 7), provide a novel insight into understanding the molecular and neuronal mechanism of STN-DBS. Even though the actual DBS mechanisms may be extraordinary complex and involve contributions of various afferents to the STN, the fact that regularization of firing patterns of STN neurons significantly

alleviates parkinsonian deficits in movement points out the importance of relative regularity of STN neuronal firing patterns in realization of normal motor function of basal ganglia.

In conclusion, our results demonstrate that histamine and the central histaminergic system is indispensable for maintaining normal STN neuronal firing patterns and basal ganglia motor functions. Our findings also provide clear evidence that DBS ameliorates parkinsonian motor symptoms by directly modulating firing patterns of STN neurons. In the light of the key position of STN neuronal firing patterns, targeting neuronal firing patterns of STN for developing new drugs as well as DBS parameter settings may help to optimize strategy for treatment of PD motor dysfunctions.

Methods

Animal model of parkinsonism and pharmacological manipulation.

Adult male Sprague-Dawley rats (~8 weeks of age, weighing 250-300 g; Experimental Animal Center of Nanjing Medical University, Nanjing, China) with either sex were used and individually housed under controlled environmental conditions (22 ± 2 ℃; 60 ± 5% humidity; and 12-h light/dark cycle with lights on at 8:00 a.m. daily). The animals were free access to standard laboratory chow and water. All rats were naive at the initiation of experiments.

We made unilateral 6-OHDA (Sigma, St. Louis, MO) lesions to establish a rat model of hemiparkinsonism. After anesthesia induced by intraperitoneal injection of sodium pentobarbital (40

mg/kg), adult rats weighing 250-300 g were placed into a stereotaxic frame (1404, David Kopf Instruments, Tujunga, CA) for the 6-OHDA injection in the medial forebrain bundle (A -4.4 mm, L 1.8 mm, and H 7.8 mm) according to the rat brain atlas of Paxinos and Watson (57) under aseptic conditions. Rats were pretreated with desipramine hydrochloride (25 mg/kg, i.p.; Sigma) 30 min before 6-OHDA injection to protect noradrenergic neurons. A stainless steel cannula (o.d. 0.5 mm, i.d. 0.3 mm) was connected by a polyethylene catheter to a 10 µl Hamilton syringe driven by an infusion pump (KDS100, KD Scientific, Holliston, MA). A total volume of 4 µl of the 6-OHDA solution (2.5 µg/µl, dissolved in saline containing 0.02% ascorbic acid, i.p.; Sigma) was then infused over a period of 4 min. The cannula was left in place for 10 min before withdrawal. Two weeks after surgery, the rats were tested for rotational behavior under injection of apomorphine (0.25 mg/kg). Only rats with prominent turning behavior (more than 25 turns in 5 minutes, see below for details) contralateral to the lesion side were considered as the parkinsonian rats, which were retained for further electrophysiological and behavioral studies. At the end of studies, TH immunostaining in the bilateral substantia nigras was conducted to identify ipsilesional dopaminergic depletion (Supplemental Figure 1).

For pharmacological manipulation, a stainless-steel guide tube (length 11 mm, o.d. 0.8 mm, i.d. 0.5 mm) for the microinjection cannulae was implanted into the STN ipsilateral to the lesion side of parkinsonian rats or bilaterally in normal rats. The lower end of the guide tube was positioned 1.8 mm above the STN (A -3.8 mm, L 2.5 mm, and H 8.0 mm), according the rat brain atlas (57). After the implantation, rats were kept on a heating pad until recovery and caged individually. During the behavioral testing sessions, one or two stainless-steel injection cannulae (length 13 mm, o.d. 0.5 mm,

i.d. 0.3 mm) was/were inserted to protrude 2 mm beyond the tip of the guide tube. Histamine (1 μg; Sigma), high K^+ (0.75 μg KCl), 2-PyEA (a selective agonist for H1 receptor; 1 μg; Sigma), dimaprit (a selective agonist for H2 receptor; 2 μg; Tocris, Bristol, UK), R-(-)-α-Methylhistamine (a selective agonist for H3 receptor; 1.5 μg; Tocris), VUF8430 (a selective agonist for H4 receptor; 3 μg; Tocris), mepyramine (a selective antagonist for H1 receptor; 4 μg; Tocris), ranitidine (a selective antagonist for H2 receptor; 3.5 μg; Tocris), JNJ5207852 (a selective antagonist for H3 receptor; 2 μg; Tocris), JNJ7777120 (a selective agonist for H4 receptor; 2.5 μg; Tocris), ZD7288 (a selective blocker for HCN channel; 3 μg; Tocris), or normal saline (0.9% NaCl) was unilaterally or bilaterally microinjected with Hamilton syringe(s) (0.5 μl each side, lasting 2 min). The effective extent of the drug diffusion in the present study was restricted in the STN according to the estimate by extracellular electrophysiological recording single unit activity of neurons located 0.05-0.6 mm away from the injection sites as we previously reported (58). Data from rats in which the injection sites were histologically identified (58, 59) to be deviated from the STN were excluded from further analysis.

Anterograde tracing with BDA.

As previously described (59-61), a glass micropipette (WPI, Sarasota, FL) with inner tip diameter of 10-15 μm was filled with 10% biotinylated dextran amine (BDA, Ref: D-1956 from Life Technologies, Carlsbad, CA) in 0.01 M phosphate buffered saline (PBS; pH 7.4) and lowered slowly into the TMN of the hypothalamus at the coordinates A -4.0 mm, L 1.6 mm, and H 9.2 mm according to the rat brain atlas (57). Iontophoresis were made under 5 μA positive alternating current

(7-s on/7-s off) for 40 min. Once completed, the micropipette was left in place for 10 min before removal. During micropipette withdrawal, the current was reversed to minimize tracer leakage through the injection tract. Rats were allowed to survive for three weeks before the terminal experiment was conducted.

Lentivirus production and injection.

To downregulate the expression of individual HCN channel subtype in the STN, four shRNA lentiviruses for *Hcn* (*Hcn1* to *Hcn4*) targeting rat HCN mRNA were constructed (Genechem, Shanghai, China). The sequences used against rat *Hcn* subtypes were as follows: *Hcn1*, GCCCGGAGACTATATCATT; *Hcn2*, CCAAGATCCTCAGTCTGCT; *Hcn3*, AGACATGGCTCGTGGTATT; *Hcn4*, GGAAGAGGATGGTGAGGAA. Recombinant lentiviruses LV-*Hcn1*-shRNA-EGFP, LV-*Hcn2*-shRNA-EGFP, LV-*Hcn3*-shRNA-EGFP, and LV-*Hcn4*-shRNA-EGFP were produced by cotransfecting 293T cells with the lentivirus expression plasmid and packaging plasmids using Lipofectamine 2000. On the other hand, to upregulate the expression of *Hcn2*, the *Hcn2* expression vector was constructed by inserting their open reading frame (ORF) sequence into the pGCL-EGFP vector. The vector containing a control shRNA for downregulation of HCN subtypes and the vector lacking an insert for overexpression of HCN2 channel were used as controls. All correct insertions were confirmed by restriction mapping and direct DNA sequencing. Transfection was performed according to the manufacture's protocol. Infectious lentiviruses were harvested 72 hours after transfection and viral titers were 1×10^9 TU/ml.

The concentrated lentivirus was delivered to the ipsilesional STN of the 6-OHDA-lesioned rat model of parkinsonism or bilaterally in normal rats using a 1 μl Hamilton syringe with a thin 25-gauge metal needle, and the injection was driven by an infusion pump (KDS100, KD Scientific; the injection volume and flow rate 1 μl at 0.1 μl/min). After the injection, the needle was left in place for 10 additional minutes and then slowly withdrawn. For parkinsonian rats, the above procedure was conducted on 7 days after 6-OHDA injection. The rats treated with lentivirus were caged individually and allowed to recover for 7 days before further electrophysiological and behavioral studies. The downregulation or upregulation of expression of HCN channel subtypes in the STN was assessed by qPCR and western blot.

Analyses of histamine and dopamine level.

The level of histamine in the STN was determined by high-performance liquid chromatography (HPLC). In brief, the tissue was homogenized in 1 mM Tris, 1 mM EGTA, 1 mM DTT, 10% sucrose, pH 7.5. After centrifugation, the supernatant was removed and a total of 10 ml of the filtrate was injected onto the analytical column. Analyses were performed on an Agilent Series 1100 liquid chromatograph (Agilent Technologies, Palo Alto, CA), equipped with a vacuum degasser, a quaternary pump, an autosampler and a diode-array detector, connected to an Agilent ChemStation software (Agilent Technologies).

In addition, the histamine level in the STN and dopamine level in the substantia nigra were quantified by competitive ELISA. In brief, the tissue was homogenized in cool PBS (4 ℃, pH 7.2).

After centrifugation, the supernatant was filter sterilized with 0.22 μm-pore-size polyvinylidene difluoride filters (Millipore, Bedford, MA). Histamine and dopamine concentration was determined using histamine (Cayman Chemical, Ann Arbor, MI) and dopamine (Biovision, Milpitas, CA) ELISA kits according to the manufacturers' instructions, respectively. Absorbance was read at 410 nm on a Biotek ELx50 spectrophotometer (Biotek, Bad Friedrichshall, Germany), and concentration was calculated using an equation generated from a standard curve.

Immunohistochemistry and stereology.

The experimental procedures for immunohistochemistry and stereology followed our previous reports (59-61). Briefly, rats were deeply anaesthetized with sodium pentobarbital (65 mg/kg) and perfused transcardially with 100 ml normal saline, followed by 250-300 ml 4% paraformaldehyde or 4% N-(3-Dimethylaminopropyl)-N'-ehylcarbodiimide hydrochloride (EDAC; Sigma; for histamine immunostaining experiment) in 0.1 M phosphate buffer. Subsequently, the brain was removed, trimmed and postfixed in the same fixative for 12 h at 4 ℃ and then cryoprotected with 30% sucrose for 48 h. For tissue processed for histamine and/or glutamate immunoreactivity, the brain was postfixed in 4% EDAC for 4 h, followed by 4% glutaraldehyde in 0.1 M phosphate buffer. Frozen coronal sections (25 μm thick) containing the STN, TMN, or substantia nigra were obtained by a freezing microtome (CM3050S, Leica, Wetzlar, Germany) and mounted on gelatin-coated slides. The slices were rinsed with 0.1 M PBS, pH 7.2 containing 0.1% Triton X-100 and then incubated in 10% normal bovine serum in PBS containing 0.1% Triton X-100 for 30 min. For glutamate

immunoreactivity, the slices were treated with 0.5% sodium borohydride in PBS for 30 min to quench autofluorescence produced by glutaraldehyde, and followed by repeated washes.

Sections were incubated overnight at 4 ℃ with primary antibody/antibodies: mouse anti-glutamate (1:1000, Millipore; Cat# MAB5304, RRID:AB_94698), goat anti-GAD67 (1:1000, Abcam, Cambridge, UK; Cat# ab80589, RRID:AB_1640532), rabbit anti-histamine (1:1000, Millipore; Cat# AB5885, RRID:AB_177540) and rabbit anti-histamine (1:500, Acris, Herford, Germany; Cat# 22939, RRID:AB_572245), mouse anti-tyrosine hydroxylase (TH) (1:2000, Sigma; Cat# T2928, RRID:AB_477569), goat anti-H1 receptor (1:500, Everest Biotech, Oxfordshire, UK; Cat# EB06904, RRID:AB_2230568) and rabbit anti-H1 receptor (1:50, Santa Cruz Biotech, Santa Cruz, CA; Cat# SC20633, RRID:AB_2277328), goat anti-H2 receptor (1:500, Everest Biotech; Cat# EB06905, RRID:AB_2121375), rabbit anti-H4 receptor (1:200, Santa Cruz Biotech; Cat# SC50313, RRID:AB_2119026), rabbit anti-HCN1 (1:300, Alomone Labs, Jerusalem, Israel; Cat# APC-056, RRID:AB_2039900), rabbit anti-HCN2 (1:100, Alomone Labs; Cat# APC-030, RRID:AB_2313726), rabbit anti-HCN3 (1:100, Alomone Labs; Cat# APC-057, RRID:AB_2039904), rabbit anti-HCN4 (1:200, Alomone Labs; Cat# APC-052, RRID:AB_2039906). These primary antibodies are validated for species and application (1DegreeBio and Antibody Registry). After a complete wash in PBS, the sections for single, double, and triple immunostaining were incubated in the related secondary antibodies (1:2000; Life Technologies) conjugated to Alexa Fluor 488, Alexa Fluor 594, and/or Alexa Fluor 350 for 2 h at room temperature in the dark. The slides were washed and mounted in Fluoromount-G mounting medium (Southern Biotech, Birmingham, AL). Incubations replacing the primary antiserum with control immunoglobulins and/or omitting the primary antiserum were used

as negative controls. All micrographs were taken with an inverted laser scanning confocal FluoView FV1000 microscope (Olympus, Tokyo, Japan), equipped with Plan-Apochromat ×60/1.42 NA oil, ×40/0.9 NA dry, ×20/0.75 NA dry, and ×10/0.4 NA dry objective lenses. Digital images from the microscope were recorded with FV10-ASW 3.1 Viewer Software (Olympus) and image processing was done with Photoshop (Adobe systems Inc, San Jose, CA) and Image Pro Plus (6.0) software (Media Cybernetics, Silver Spring, MD).

The number of the dopaminergic neurons in the substantia nigra pars compacta and the EGFP-positive glutamatergic neurons (in which HCN channels were selectively downregulated or upregulated by lentivirus vectors) in the STN were quantified by the numerical density, which was estimated by counting the number of neurons within three dimensional optical dissectors that were systematically spaced at random throughout the selected brain areas. Ten optical dissectors sized 100 × 100 × 50 μm were randomly sampled, and the number of positive cells in each dissector was quantified. The density of cells was estimated using the formula: Nv = Q/v (dis), where Q is the average number of cells counted per dissector, and v (dis) is the volume of the dissector: v (dis) = a [frame] × h, where ‘a’ is area of frame and ‘h’ is dissector height. Data were represented as the number of cells per cubic millimeter. The histaminergic fiber density in STN was measured by calculation of areas covered with fibers in 20 optical dissectors sized 100 × 100 μm that were systematically spaced at random throughout the STN.

qPCR on tissue punches and single-cell qPCR.

qPCR on tissue punches and single-cell qPCR were performed as previously described (30, 58). For quantification, the quantity of the target gene was expressed relative to the amount of the reference gene (*Gapdh*) to obtain a normalized target expression value. For negative controls, cDNA was replaced with water. Primer sequences were summarized in Supplemental Table 1.

For single-cell qPCR, after whole-cell patch clamp recordings, the content of the recorded neuron was aspirated into the recording pipette and expelled into Single Cell Lysis/Dnase I solution using the Single Cell-to-CTTM Kit (Life Technologies). Reverse transcription and cDNA pre-amplification were performed on ABI QuantStudio 6 Flex on Quantstudio™ 6 Flex (Life Technologies) according to the kit protocol. qPCR was performed using the TaqMan Gene Expression Assay system. The TaqMan assay probes were designed and purchased from Life Technologies: Rn00566691_s1 for *Hrh1*, Rn00564216_s1 for *Hrh2*, Rn00585276_m1 for *Hrh3*, Rn00590929_m1 for *Hrh4*, Rn00670384_m1 for *Hcn1*, Rn01408572_mH for *Hcn2*, Rn00586666_m1 for *Hcn3*, Rn00572232_m1 for *Hcn4*, Rn01775763_g1 for *Gapdh*. Conditions for the cycles followed the manufacturer's protocol for TaqMan assays. A negative control was obtained from clean pipettes containing internal solution. Results were analyzed by using Real-Time StatMiner software (Integromics TM, Philadelphia, PA).

Western blot.

STN tissue punches were homogenized in 200 µl of lysis buffer (1% Nonidet P-40, 20 mM Tris, pH 8.0, 137 mM NaCl, 10% glycerol, 1 mM PMSF, sodium butyrate 1 mM, and protease inhibitors)

at 4 ℃. After removal of cellular debris by centrifugation, the supernatant was collected, and protein levels were measured by the Bradford assay (Bio-Rad, Hercules, CA). 20 μg of each sample was boiled in the presence of sample buffer for 5 min before separation on 10% SDS polyacrylamide gel, and proteins were transferred to nitrocellulose membranes. The immunoblots were blocked with 5% milk in TBS for 60 min. The membranes were then incubated overnight at 4 ℃ with primary antibody: rabbit anti-HCN1 (1:500, Alomone labs), rabbit anti-HCN2 (1:200, Alomone labs), rabbit anti-HCN3 (1:200, Alomone labs), or rabbit anti-HCN4 (1:300, Alomone labs). Primary antibody incubation was followed by three washes (5 min, rocking, room temperature) in TBST (TBS containing 0.2% Tween 20) before incubation with the secondary antibody (HRP-conjugated goat anti-rabbit IgG (H+L) secondary antibody; Thermo Scientific, Waltham, MA), three washes. The protein-antibody complexes were visualized by the Pierce ECL Western Blotting Substrate (Thermo Scientific) and exposed to Kodak medical X-ray film (Denville Scientific Inc, Holliston, MA). GAPDH was used as a loading control. The optical densities of protein bands were quantitatively analyzed with Quantity One software (Bio-Rad).

Multielectrode array recordings in vivo.

To record the extracellular neuronal activities of STN in vivo, elliptic microwire recording arrays (~ 0.628 mm^2; Stablohm 675, Formvar natural coated, CA Fine Wire, Grover Beach, CA), constructed of 14 microwires for recording and a pair of bipolar/twisted electrode (stainless steel, Teflon coated, 100 μm in diameter) in the center for stimulation, were used and targeted at ipsilesional STN (A -3.4--3.9 mm, L 2.2-2.8 mm, and H 7.3-8.3 mm) in parkinsonian rats, according

to the rat brain atlas (57). An additional ground wire was connected to the stainless steel screw for reference, which was firmly attached to the skull.

Single-unit neuronal activity was recorded using a data acquisition system (Cerebus, Blackrock Microsystems, Salt Lake City, UT). The STN neuronal discharges were detected by the electrode array and passed from the headstage assemblies to the amplifier. The STN was identified by its highly typical firing properties distinguished from cells of the overlying zona incerta and the underlying cerebral peduncle. Penetration of the electrode tip into the STN is characterized by a sudden increase in single unit activity of spontaneously active neurons, and the exit of electrode tip out of the STN corresponds to a loss of single cell activity (10, 62). The analog signals were amplified and filtered at cut-off frequencies of 0.3 Hz and 7.5 kHz. The signals from each microelectrode were further filtered (250 Hz to 5 kHz), and continuously digitized and saved to disk at a rate of 30 kHz. Then, the recorded data were analyzed by Spike 2 (CED, Cambridge, UK) and NeuroExplorer (MicroBrightField, Williston, VT). Only single units with clear separation from the noise cluster were used for further analysis. Spike waveforms were sorted, using a combination of automatic and manual sorting techniques. Automatic clustering techniques (K-means clustering and valley seeking methods) were used to produce an initial separation of waveforms into individual cluster. Each cluster was then checked manually to ensure that the cluster boundaries were well separated and spike waveforms were consistent. A group of similar waveforms was considered as being generated from a single neuron. The peristimulus time histograms (PSTHs; bin width 1 s) of neuronal discharges were generated to assess the changes in firing rate of STN neurons. The autocorrelograms of unit activity (bin width 1 ms) and smoothed with Gaussian filter (the middle

curve), inter-spike interval (ISI) time series (scatterplot), and ISI distributions (bin width 1 ms) were generated to analyze firing pattern. Firing bursts were defined by the following parameters: maximal interval at start of a burst: 200 ms; maximal inter-spike interval in a burst: 400 ms; minimal duration of a burst: 100 ms; minimal interval between bursts: 200 ms; minimal number of spikes in a burst: 3. The coefficient of variation (CV) of ISI, the number of burst and the inter-burst intervals during the period between 90 s before and 90 s after maximal firing rate were counted and calculated for assessing the degree of regularization of firing pattern.

The local field potentials were simultaneously recorded through recording electrodes. STN oscillatory rhythm was analyzed using NeuroExplorer software. Power spectral density was built to observe the power distribution under different conditions. The spectrum value was normalized as log of raw power spectral density from 0.5 to 100 Hz, which was calculated using Fast Fourier Transform with Hanning window function, shifting each 0.05 s without overlap. The frequency block was set at 512 at 0.2 Hz resolution.

Patch clamp recordings in vitro.

Whole-cell patch clamp and cell-attached recordings were performed as previously described (58, 59, 63) on STN neurons on brain slices to assess the receptor and ionic mechanisms. Cell-attached recordings were carried out to analyze firing rate and firing pattern without rupturing the cell membrane. The ACSF used for whole-cell patch clamp recordings (composed in mM): 124 NaCl, 2.5 KCl, 1.25 NaH_2PO_4, 1.3 $MgSO_4$, 26 $NaHCO_3$, 2 $CaCl_2$ and 20 D-glucose; for cell-attached

recordings: 124 NaCl, 5 KCl, 1.25 KH_2PO_4, 1.3 $MgSO_4$, 26 $NaHCO_3$, 2.4 $CaCl_2$ and 10 D-glucose; for high potassium in whole-cell patch clamp recordings (substituting part of the KCl with equimolar NaCl): 120.25 NaCl, 8.75 KCl, 1.25 KH_2PO_4, 1.3 $MgSO_4$, 26 $NaHCO_3$, 2.4 $CaCl_2$ and 10 D-glucose.

STN neurons were visualized with an Olympus BX51WI microscope (Tokyo, Japan) equipped with infrared differential interference contrast. Whole-cell patch clamp and cell-attached recordings were acquired with an Axopatch-700B amplifier (Axon Instruments, Sunnyvale, CA) and the signals were fed into the computer through a Digidata-1550 interface (Axon Instruments) for data capture and analysis (pClamp 10.0, Axon Instruments). We bathed the slices with histamine (0.3-30 μM) and high K^+ to stimulate the recorded STN neurons. Before bath application, the whole-cell current or spontaneous firing rate of the recorded neuron was observed for at least 20 min to assure stability. Then, histamine or high K^+ was added to the perfusing ACSF to stimulate the recorded neuron for a test period of 1 min. After each stimulation, cells were given at least 20 min for recovery and prevention of desensitization. TTX (0.3 μM, Alomone Labs), selective non-NMDA receptor antagonist CNQX (20 μM, Tocris), selective NMDA receptor antagonist AP5 (50 μM, Tocris), and selective $GABA_A$ receptor antagonist SR 95531 (50 μM, Tocris) was used to determine whether the effect of histamine is postsynaptic. Selective agonists for histamine receptor subtypes, 2-PyEA (30 μM), dimaprit (30 μM), and VUF8430 (30 μM), as well as selective antagonists, mepyramine (1 μM), ranitidine (1 μM), or JNJ7777120 (10 μM) was applied to examine the underlying postsynaptic receptor mechanism. The receptor antagonist or ion channel blocker was given for at least 15 min before we observed their effects.

To characterize the histamine-induced whole-cell current, in voltage-clamp recording, current-voltage plots (*I-V* curves) were obtained before and during histamine application using a slow ramp command (dV/dt = -10 mV s^{-1}, ranged from -60 to -130 mV) to allow for attainment of steady-state conditions (58, 59). In addition, depolarizing voltage sag generated by activation of the HCN channels in response to a hyperpolarizing current stimulation (80-150 pA, 1 s) in the absence and presence of histamine was measured in current-clamp recordings. The amplitude of voltage sag was calculated by subtracting the peak voltage amplitude from the steady-state voltage, and ZD7288 (50 μM) was applied to block HCN channels. Moreover, to examine the effect of histamine on the HCN channel current (I_h), *I-V* curves were obtained before and during histamine application using a series of 1 s hyperpolarizing voltage steps (ranging from -50 to -120 mV in 10 mV steps) (64). I_h was determined by subtracting instantaneous current (I_{Ins}) from maximum current at 1 s ($I_{Max-1ms}$) at each hyperpolarizing voltage step using the following equation: $I_h = I_{Max-1ms} - I_{Ins}$. I_h conductance (G_h) was estimated as the amplitude of I_h measured at various potentials (V) divided by the driving force ($V–E_h$): $G_h = I_h / (V - E_h)$, where E_h is the reversal potential of I_h determined by clamping STN neurons to -120 mV for 1 s and depolarizing in 10 mV at 1-s increments to -50 mV. G was normalized to maximum, and fitted with the modified Boltzmann function: $G_{norm} = 1/(1 + \exp((V - V_{1/2})/k))$, where G_{norm} is the fraction of maximal G_h observed at V, $V_{1/2}$ is the voltage required for half-maximal activation, and k is the slope factor.

DBS of STN.

A pair of bipolar/twisted stimulating electrode (stainless steel, Teflon coated, 100 μm in diameter) in the center of elliptic microwire recording arrays (~ 0.628 mm^2; Stablohm 675, Formvar natural coated, CA Fine Wire), constructed of 14 microwires for recording was implanted stereotaxically into the ipsilesional STN (A -3.6 mm, L 2.5 mm, and H 8.0 mm), with the guidance of electrophysiological recordings for the highly typical firing properties of STN neurons as described in the *Multielectrode array recordings in vivo*. Electrical rectangular stimulation was applied to STN by using a Master-9 stimulator (AMPI, Jerusalem, Israel). Stimulation parameters were as follows: frequency, 125 Hz; intensity, 70 μA; pulse width, 80 μs; and stimulation time, 5 min (11).

In vivo microdialysis sampling.

In vivo microdialysis sampling of histamine was performed on freely moving 6-OHDA-lesioned animals. The microdialysis probe had an 8.0 mm shaft with a 1.0 mm, 50 kD molecular weight cutoff polyethylene membrane (DZ-9-01, Eicom, Kyoto, Japan). Before use, the probe was washed with ACSF. The preconditioned probe's inlet was connected to a microsyringe pump (ESP-32, Eicom), using fluorinated ethylene propylene tubing. Probe implantation was performed on anesthetized animals 10 days post-lesion. Rats were stereotactically implanted with a guide cannula at a 20-degree angle (caudorostral to the vertical plane) into the ipsilesional STN (A -3.6 mm, L 2.5 mm, and H 8.0 mm). Four days after surgery, the rats were placed in an open field, and a probe was inserted through the guide. The probe was perfused with ACSF for 240 min at a flow rate of 10 μl/min before sample collection. Samples (50 μl) were collected at a flow rate of 0.5

μl/min and kept at 4℃ (EFR-82 Cooling Unit; Eicom) and each hour they were transferred to a -80℃ freezer and stored until analyzed.

Behavioral tests.

The animals used in behavioral tests were randomly grouped by different treatments according to a random number table. All behavioral tests started at the same time (10:00 a.m.) each day. The experimenter performing the behavioral tests was blind to the treatment groups and the side of dopamine depletion. In order to achieve a stable motor performance in the adhesive removal, accelerating rota-rod and balance beam tests, each animal was trained daily for at least 10 trials for 3 to 5 consecutive days before tests as we previously reported (58, 59).

Turning behavior test. The 6-OHDA-lesioned animals were given apomorphine (0.25 mg⁄ kg, i.p.) and placed individually into a 30-cm-diameter round bowl. The number of rotation contralateral to the lesion side was counted during a 30-min interval after apomorphine injection.

The adhesive removal test. This test is considered as an evaluation of motor initiation and execution (65). Prior to surgery, two training trials were performed by placing two adhesive tapes (8 mm × 6 mm) on the plantar surface of both forelimbs simultaneously. The rat may bring one forelimb onto the other forelimb and use its mouth to remove the adhesives. We training the animals by performing 1 trial per animal per day for 5 days (each trial elapsed a maximum of 3 min) on 10 days post-surgery. At day 15 after 6-OHDA or saline injections, adhesive dots were placed on both

forelimbs and the time to remove the tape was recorded. If a rat did not remove either or both stickers within 60 s, the animal received a score of 60 s.

Footprints. We assessed walking pattern and gait kinematics by a footprint test (59). Rat hindpaws were painted with nontoxic inks, and the rats were allowed to spontaneously traverse a clear plexiglass tunnel (100 cm × 10 cm × 10 cm) ending in a darkened cage. A sheet of white absorbent paper (100 cm × 10 cm) was placed at the bottom of the track. The resulting tracks provide the spatial relationship of consecutive footfalls from which the stride length and width were measured.

Balance beam test. We evaluated motor balance and coordination by measuring the ability of the animals traverse a balance beam of 190 cm in length and a diameter of 2.5 cm. A plastic platform (7 cm × 4 cm) was placed at one end of the rod as the start, and a black plastic box (15 cm × 15 cm × 8 cm) was set at the other end of the rod as a nest for motivating the animal to cross the beam. The apparatus was suspended 90 cm above a cushion, which protected the fallen animals from injury, and 50 cm from a wall. Each animal was trained daily for at least 10 trials for 3-5 consecutive days in order to achieve a stable performance on the balance beam. The time taken to traverse the beam was recorded. The test consisted of 5 consecutive trails. To reduce stress and fatigue, the animals were allowed a 90 s rest between trials.

Accelerating rota-rod test. To assess motor coordination and balance, we used a commercially available accelerating rota-rod (47750, Ugo Basile, Varese, Italy). Animals were first habituated to

low rotation (4 rpm) for 30 s, and then the rod was evenly accelerated up to 40 rpm during 300 s (acceleration was 0.12 rpm/s). The time taken for the rat to fall from the rotating rod was recorded, and the time beyond 300 s was recorded as 300 s. Each animal was trained daily for at least 10 trials for 3-5 consecutive days in order to achieve a stable performance on the accelerating rota-rod. For the test, each rat was subjected three trials, with a 3-min resting interval to reduce stress and fatigue.

Open field test. An open field arena (50 cm × 50 cm × 50 cm) was used to assess spontaneous motor activity. The spontaneous locomotor activity was monitored by a video camera, and the total movement distance traveled during five minutes were quantified by Clever TopScan (Clever Sys, Reston, VA).

Statistical analysis.

All data were analyzed with SPSS 17.0 (SPSS, Chicago, IL). Data were tested for normal distribution and homogeneity of variance. Two-tailed Student's t test, one-way, two-way, and repeated measures two-way analysis of variance (ANOVA), and Newman-Keuls post hoc testing were employed for statistical analysis. *P*-values of < 0.05 were considered to be significant. The detailed statistical results for each experiment were summarized in Supplemental Table 2.

Study approval

All experiments were carried out in accordance with the U.S. National Institutes of Health Guide for the Care and Use of Laboratory Animals (NIH Publication 85-23, revised 2011) and were approved by the Experimental Animal Care and Use Committee of Nanjing University. All efforts were made to minimize the number of animals used and their suffering.

Author Contributions:

J.-N.Z and J.-J.W. conceived and designed the study. Q.-X.Z. performed tracing, immunostaining, qPCR, western blot, HPLC, ELISA and patch clamp recording experiments. G.-Y.L. performed behavioral experiments. B.L. performed multielectrode array recording and behavioral experiments. C.-Z.Z. and K.X. was involved in behavioral experiments. H.-Z.L. was involved in electrophysiological experiments. Q.-X.Z., G.-Y.L., B.L. and X.-Y.Z. analyzed data. J.-N.Z and J.-J.W. wrote the paper.

Acknowledgements:

This work was supported by the National Natural Science Foundation of China (grants 31330033, 81671107, 31471112, 91332124, 31771143, 31500848, 31600834, and NSFC/RGC Joint Research Scheme 31461163001); the Ministry of Education of China (SRFDP/RGC ERG grant 20130091140003, NCET program, and Fundamental Research Funds for the Central Universities 020814380071 and 020814380091); and the Natural Science Foundation of Jiangsu Province, China (grants BK2011014, BK20140599 and BK20151384).

References

1. Benabid AL, Chabardes S, Mitrofanis J, and Pollak P. Deep brain stimulation of the subthalamic nucleus for the treatment of Parkinson's disease. *Lancet Neurol.* 2009;8(1):67-81.
2. Eisenstein M. Electrotherapy: Shock value. *Nature.* 2016;538(7626):S10-S2.
3. DeLong MR. Primate models of movement disorders of basal ganglia origin. *Trends Neurosci.* 1990;13(7):281-5.
4. Parent A, and Hazrati LN. Functional anatomy of the basal ganglia. II. The place of subthalamic nucleus and external pallidum in basal ganglia circuitry. *Brain Res Rev.* 1995;20(1):128-54.
5. Calabresi P, Picconi B, Tozzi A, Ghiglieri V, and Di Filippo M. Direct and indirect pathways of basal ganglia: a critical reappraisal. *Nat Neurosci.* 2014;17(8):1022-30.
6. Nambu A, Tokuno H, and Takada M. Functional significance of the cortico-subthalamo-pallidal 'hyperdirect' pathway. *Neurosci Res.* 2002;43(2):111-7.
7. Chu HY, Atherton JF, Wokosin D, Surmeier DJ, and Bevan MD. Heterosynaptic regulation of external globus pallidus inputs to the subthalamic nucleus by the motor cortex. *Neuron.* 2015;85(2):364-76.
8. Chu HY, McIver EL, Kovaleski RF, Atherton JF, and Bevan MD. Loss of Hyperdirect Pathway Cortico-Subthalamic Inputs Following Degeneration of Midbrain Dopamine Neurons. *Neuron.* 2017;95(6):1306-18 e5.
9. Plenz D, and Kital ST. A basal ganglia pacemaker formed by the subthalamic nucleus and external globus pallidus. *Nature.* 1999;400(6745):677-82.
10. Gradinaru V, Mogri M, Thompson KR, Henderson JM, and Deisseroth K. Optical deconstruction of parkinsonian neural circuitry. *Science.* 2009;324(5925):354-9.
11. Li Q, Ke Y, Chan DC, Qian ZM, Yung KK, Ko H, et al. Therapeutic deep brain stimulation in Parkinsonian rats directly influences motor cortex. *Neuron.* 2012;76(5):1030-41.
12. Sharott A, Gulberti A, Zittel S, Tudor Jones AA, Fickel U, Munchau A, et al. Activity parameters of subthalamic nucleus neurons selectively predict motor symptom severity in Parkinson's disease. *J Neurosci.* 2014;34(18):6273-85.
13. Yang AI, Vanegas N, Lungu C, and Zaghloul KA. Beta-coupled high-frequency activity and beta-locked neuronal spiking in the subthalamic nucleus of Parkinson's disease. *J Neurosci.* 2014;34(38):12816-27.
14. Huebl J, Spitzer B, Brucke C, Schonecker T, Kupsch A, Alesch F, et al. Oscillatory subthalamic nucleus activity is modulated by dopamine during emotional processing in Parkinson's disease. *Cortex.* 2014;60:69-81.
15. Cagnan H, Duff EP, and Brown P. The relative phases of basal ganglia activities dynamically shape effective connectivity in Parkinson's disease. *Brain.* 2015;138(Pt 6):1667-78.
16. Wang DD, de Hemptinne C, Miocinovic S, Qasim SE, Miller AM, Ostrem JL, et al. Subthalamic local field potentials in Parkinson's disease and isolated dystonia: An evaluation of potential biomarkers. *Neurobiol Dis.* 2016;89:213-22.
17. Bergman H, Wichmann T, and DeLong MR. Reversal of experimental parkinsonism by lesions of the subthalamic nucleus. *Science.* 1990;249(4975):1436-8.
18. Escobar Sanabria D, Johnson LA, Nebeck SD, Zhang J, Johnson MD, Baker KB, et al. Parkinsonism and vigilance: alteration in neural oscillatory activity and phase-amplitude coupling in the basal ganglia and motor cortex. *J Neurophysiol.* 2017;118(5):2654-69.
19. Chan CS, Glajch KE, Gertler TS, Guzman JN, Mercer JN, Lewis AS, et al. HCN channelopathy in external globus pallidus neurons in models of Parkinson's disease. *Nat Neurosci.* 2011;14(1):85-92.

20. Delaville C, McCoy AJ, Gerber CM, Cruz AV, and Walters JR. Subthalamic nucleus activity in the awake hemiparkinsonian rat: relationships with motor and cognitive networks. *J Neurosci.* 2015;35(17):6918-30.
21. Pan MK, Kuo SH, Tai CH, Liou JY, Pei JC, Chang CY, et al. Neuronal firing patterns outweigh circuitry oscillations in parkinsonian motor control. *J Clin Invest.* 2016;126(12):4516-26.
22. Rinne JO, Anichtchik OV, Eriksson KS, Kaslin J, Tuomisto L, Kalimo H, et al. Increased brain histamine levels in Parkinson's disease but not in multiple system atrophy. *J Neurochem.* 2002;81(5):954-60.
23. Anichtchik OV, Peitsaro N, Rinne JO, Kalimo H, and Panula P. Distribution and modulation of histamine H(3) receptors in basal ganglia and frontal cortex of healthy controls and patients with Parkinson's disease. *Neurobiol Dis.* 2001;8(4):707-16.
24. Panula P, and Nuutinen S. The histaminergic network in the brain: basic organization and role in disease. *Nat Rev Neurosci.* 2013;14(7):472-87.
25. Haas H, and Panula P. The role of histamine and the tuberomamillary nucleus in the nervous system. *Nat Rev Neurosci.* 2003;4(2):121-30.
26. Haas HL, Sergeeva OA, and Selbach O. Histamine in the nervous system. *Physiol Rev.* 2008;88(3):1183-241.
27. Sutcliffe JG, and de Lecea L. Not asleep, not quite awake. *Nat Med.* 2004;10(7):673-4.
28. Eban-Rothschild A, Giardino WJ, and de Lecea L. To sleep or not to sleep: neuronal and ecological insights. *Curr Opin Neurobiol.* 2017;44:132-8.
29. Zhu JN, Yung WH, Kwok-Chong Chow B, Chan YS, and Wang JJ. The cerebellar-hypothalamic circuits: potential pathways underlying cerebellar involvement in somatic-visceral integration. *Brain Res Rev.* 2006;52(1):93-106.
30. Zhang J, Zhuang QX, Li B, Wu GY, Yung WH, Zhu JN, et al. Selective Modulation of Histaminergic Inputs on Projection Neurons of Cerebellum Rapidly Promotes Motor Coordination via HCN Channels. *Mol Neurobiol.* 2016;53(2):1386-401.
31. Bolam JP, and Ellender TJ. Histamine and the striatum. *Neuropharmacology.* 2016;106:74-84.
32. Shan L, Dauvilliers Y, and Siegel JM. Interactions of the histamine and hypocretin systems in CNS disorders. *Nat Rev Neurol.* 2015;11(7):401-13.
33. Kravitz AV, Freeze BS, Parker PR, Kay K, Thwin MT, Deisseroth K, et al. Regulation of parkinsonian motor behaviours by optogenetic control of basal ganglia circuitry. *Nature.* 2010;466(7306):622-6.
34. Hutchison WD, Allan RJ, Opitz H, Levy R, Dostrovsky JO, Lang AE, et al. Neurophysiological identification of the subthalamic nucleus in surgery for Parkinson's disease. *Ann Neurol.* 1998;44(4):622-8.
35. Kass JI, and Mintz IM. Silent plateau potentials, rhythmic bursts, and pacemaker firing: three patterns of activity that coexist in quadristable subthalamic neurons. *Proc Natl Acad Sci U S A.* 2006;103(1):183-8.
36. Tai CH, Yang YC, Pan MK, Huang CS, and Kuo CC. Modulation of subthalamic T-type Ca(2+) channels remedies locomotor deficits in a rat model of Parkinson disease. *J Clin Invest.* 2011;121(8):3289-305.
37. Pape HC. Queer current and pacemaker: the hyperpolarization-activated cation current in neurons. *Annu Rev Physiol.* 1996;58:299-327.
38. Ludwig A, Zong X, Jeglitsch M, Hofmann F, and Biel M. A family of hyperpolarization-activated mammalian cation channels. *Nature.* 1998;393(6685):587-91.
39. Seifert R, Scholten A, Gauss R, Mincheva A, Lichter P, and Kaupp UB. Molecular characterization of a slowly gating human hyperpolarization-activated channel predominantly expressed in thalamus, heart, and testis. *Proc Natl Acad Sci U S A.* 1999;96(16):9391-6.
40. Biel M, Wahl-Schott C, Michalakis S, and Zong X. Hyperpolarization-activated cation channels: from genes to function. *Physiol Rev.* 2009;89(3):847-85.

41. Chen X, Sirois JE, Lei Q, Talley EM, Lynch C, 3rd, and Bayliss DA. HCN subunit-specific and cAMP-modulated effects of anesthetics on neuronal pacemaker currents. *J Neurosci.* 2005;25(24):5803-14.
42. Limousin P, Pollak P, Benazzouz A, Hoffmann D, Le Bas JF, Broussolle E, et al. Effect of parkinsonian signs and symptoms of bilateral subthalamic nucleus stimulation. *Lancet.* 1995;345(8942):91-5.
43. Miocinovic S, Somayajula S, Chitnis S, and Vitek JL. History, applications, and mechanisms of deep brain stimulation. *JAMA Neurol.* 2013;70(2):163-71.
44. Hammond C, Bergman H, and Brown P. Pathological synchronization in Parkinson's disease: networks, models and treatments. *Trends Neurosci.* 2007;30(7):357-64.
45. McCarthy MM, Moore-Kochlacs C, Gu X, Boyden ES, Han X, and Kopell N. Striatal origin of the pathologic beta oscillations in Parkinson's disease. *Proc Natl Acad Sci U S A.* 2011;108(28):11620-5.
46. Brocker DT, Swan BD, So RQ, Turner DA, Gross RE, and Grill WM. Optimized temporal pattern of brain stimulation designed by computational evolution. *Sci Transl Med.* 2017;9(371).
47. Atherton JF, Menard A, Urbain N, and Bevan MD. Short-term depression of external globus pallidus-subthalamic nucleus synaptic transmission and implications for patterning subthalamic activity. *J Neurosci.* 2013;33(17):7130-44.
48. Li GY, Zhuang QX, Li B, Wang JJ, and Zhu JN. Subthalamic nucleus: from circuits, functions to a deep brain stimulation target for the treatment of Parkinson's disease. *Acta Physiol Sin.* 2017;69(5):611-22.
49. Levy R, Lang AE, Dostrovsky JO, Pahapill P, Romas J, Saint-Cyr J, et al. Lidocaine and muscimol microinjections in subthalamic nucleus reverse Parkinsonian symptoms. *Brain.* 2001;124(Pt 10):2105-18.
50. Benedetti F, Colloca L, Torre E, Lanotte M, Melcarne A, Pesare M, et al. Placebo-responsive Parkinson patients show decreased activity in single neurons of subthalamic nucleus. *Nat Neurosci.* 2004;7(6):587-8.
51. Lang AE, and Obeso JA. Challenges in Parkinson's disease: restoration of the nigrostriatal dopamine system is not enough. *Lancet Neurol.* 2004;3(5):309-16.
52. Tiligada E, Kyriakidis K, Chazot PL, and Passani MB. Histamine pharmacology and new CNS drug targets. *CNS Neurosci Ther.* 2011;17(6):620-8.
53. Atherton JF, Kitano K, Baufreton J, Fan K, Wokosin D, Tkatch T, et al. Selective participation of somatodendritic HCN channels in inhibitory but not excitatory synaptic integration in neurons of the subthalamic nucleus. *J Neurosci.* 2010;30(47):16025-40.
54. Chetrit J, Taupignon A, Froux L, Morin S, Bouali-Benazzouz R, Naudet F, et al. Inhibiting subthalamic D5 receptor constitutive activity alleviates abnormal electrical activity and reverses motor impairment in a rat model of Parkinson's disease. *J Neurosci.* 2013;33(37):14840-9.
55. Ludwig A, Budde T, Stieber J, Moosmang S, Wahl C, Holthoff K, et al. Absence epilepsy and sinus dysrhythmia in mice lacking the pacemaker channel HCN2. *EMBO J.* 2003;22(2):216-24.
56. Tan H, Pogosyan A, Ashkan K, Cheeran B, FitzGerald JJ, Green AL, et al. Subthalamic nucleus local field potential activity helps encode motor effort rather than force in parkinsonism. *J Neurosci.* 2015;35(15):5941-9.
57. Paxinos G, and Watson C. *The rat brain in stereotaxic coordinates.* San Diego: Academic Press; 2014.
58. Zhang J, Li B, Yu L, He YC, Li HZ, Zhu JN, et al. A role for orexin in central vestibular motor control. *Neuron.* 2011;69(4):793-804.
59. Wang Y, Chen ZP, Zhuang QX, Zhang XY, Li HZ, Wang JJ, et al. Role of Corticotropin-Releasing Factor in Cerebellar Motor Control and Ataxia. *Curr Biol.* 2017;27(17):2661-9 e5.
60. Li B, Zhuang QX, Gao HR, Wang JJ, and Zhu JN. Medial cerebellar nucleus projects to feeding-related neurons in the ventromedial hypothalamic nucleus in rats. *Brain Struct Funct.* 2017;222(2):957-71.
61. Ji MJ, Zhang XY, Chen Z, Wang JJ, and Zhu JN. Orexin prevents depressive-like behavior by promoting stress resilience. *Mol Psychiat.* 2018; doi: 10.1038/s41380-018-0127-0.

62. Perier C, Tremblay L, Feger J, and Hirsch EC. Behavioral consequences of bicuculline injection in the subthalamic nucleus and the zona incerta in rat. *J Neurosci.* 2002;22(19):8711-9.
63. Dugladze T, Schmitz D, Whittington MA, Vida I, and Gloveli T. Segregation of axonal and somatic activity during fast network oscillations. *Science.* 2012;336(6087):1458-61.
64. Friedman AK, Walsh JJ, Juarez B, Ku SM, Chaudhury D, Wang J, et al. Enhancing depression mechanisms in midbrain dopamine neurons achieves homeostatic resilience. *Science.* 2014;344(6181):313-9.
65. Bouet V, Boulouard M, Toutain J, Divoux D, Bernaudin M, Schumann-Bard P, et al. The adhesive removal test: a sensitive method to assess sensorimotor deficits in mice. *Nat Protoc.* 2009;4(10):1560-4.

Figures

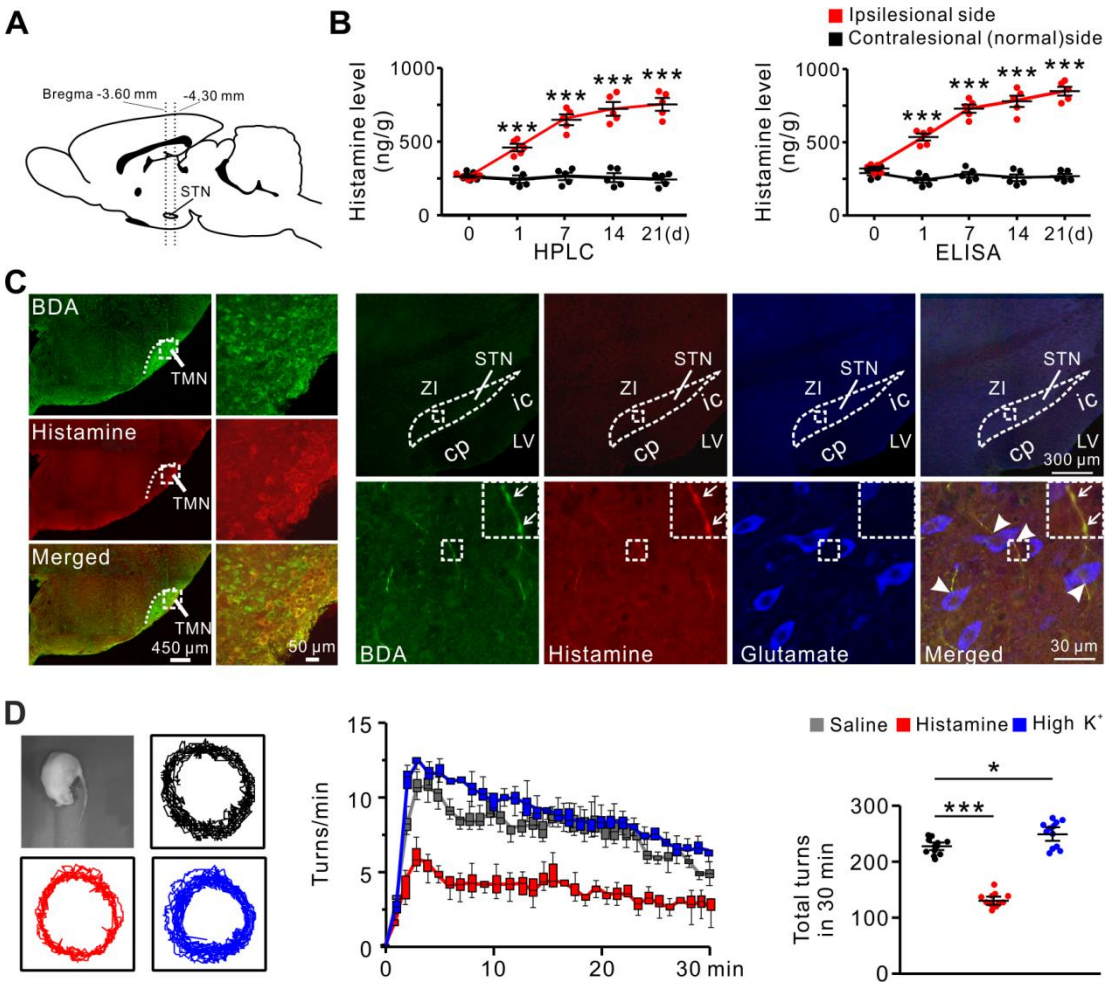

Figure 1. Histaminergic afferents in the STN and the histamine-induced amelioration of turning behavior of PD rats. (**A**) Sagittal view of the rat brain showing the localization of the STN between -3.60 and -4.30 mm from the Bregma. STN tissue punches for analysis of histamine levels were collected from brain slices obtained using these coordinates. (**B**) HPLC and ELISA analyses show levels of histamine (ng/g of tissue) in the ipsilesional and contralesional STN of PD rats (n = 10) on 1, 7, 14 and 21 days after 6-OHDA injection (*n* = 5). (**C**) Immunofluorescence staining shows that anterogradely labeled BDA fibers in the STN, originating from the histaminergic neurons in the hypothalamic TMN (left panel), contained histamine immunoreactivity (right pannel). Note that

these histaminergic fibers possessed prominent varicosities (indicated by arrows) and passed around (indicated by arrowheads) glutamate immunoreactive (glutamatergic) neurons in the STN (3 independent experiments). cp, cerebral peduncle; ic, internal capsule; LV, lateral ventricle; TMN, tuberomammillary nucleus of the hypothalamus; ZI, zona incerta. (**D**) Behavioral tests show that histamine (1 μg) microinjected into STN decreased, whereas high K^+ (0.75 μg KCl) increases, the rate and total number of apomorphine-induced turnings in 30 min in PD rats (n = 12). Data are represented as mean ± SEM or median (horizontal bar) with 25th-75th (box) and 5th-95th (whiskers) percentiles; ns, no statistical difference, * $P < 0.05$ and *** $P < 0.001$ by two-way (**B**) or one-way ANOVA (**D**) with Newman-Keuls post hoc test.

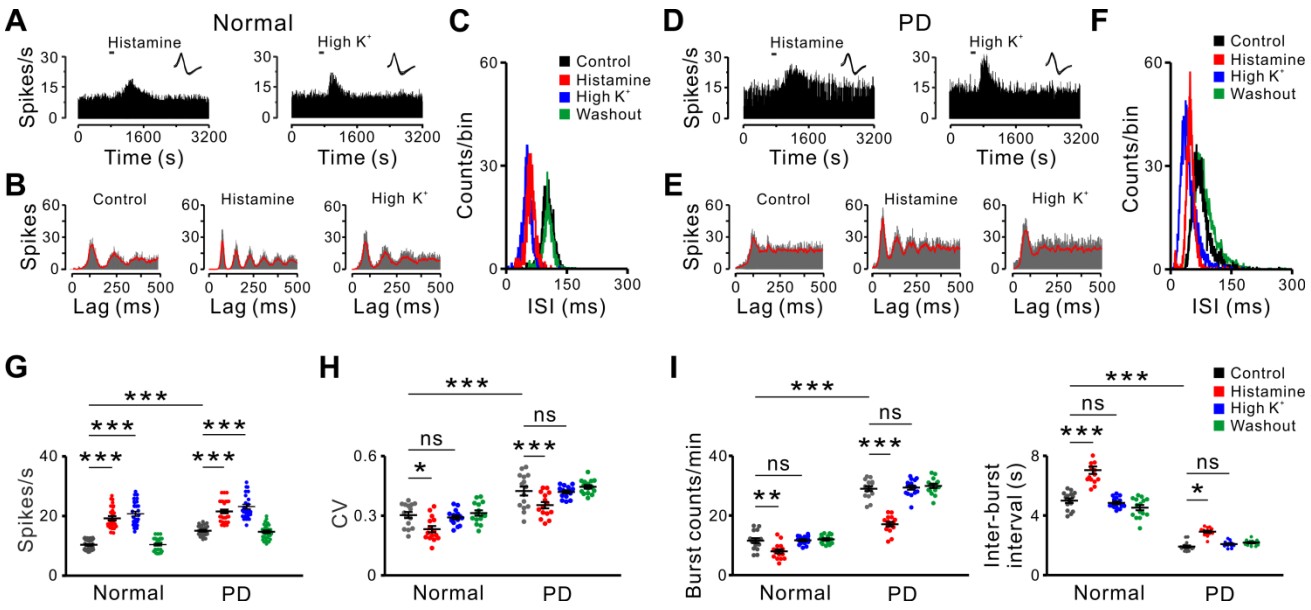

Figure 2. The histamine-induced regularization of firing patterns of STN neurons in normal and PD rats. (**A-F**) Effects of histamine (1 μg) and high K^+ (0.75 μg KCl) on firing rate and firing pattern of two recorded STN neurons in a normal and PD rats in vivo. PSTHs (**A** and **D**) show that both histamine and high K^+ excited the STN neuron. The insets represent five superimposed traces of spike waveforms for each unit, respectively. Autocorrelation histograms (**B** and **E**) show that histamine, rather than high K^+, promoted periodicity of STN neuronal firing. ISI histograms (**C** and **F**) show that histamine but not high K^+ narrowed ISI distributions. (**G-I**) Histamine increased the firing rates (**G,** n = 30), decreased CV of ISIs (**H,** n = 15), reduced the number of bursts (**I**, left panel, n = 15), and prolonged the inter-burst intervals (**I**, right panel, n = 15) of STN neurons in both normal and PD rats. However, high K^+ only increased the firing rates (**G**) but did not influence the firing patterns (**H** and **I**) of STN neurons in normal and PD rats. Data are represented as mean ± SEM; ns, no statistical difference, * $P < 0.05$, ** $P < 0.01$, and *** $P < 0.001$ by two-way ANOVA with Newman-Keuls post hoc test (**G-I**).

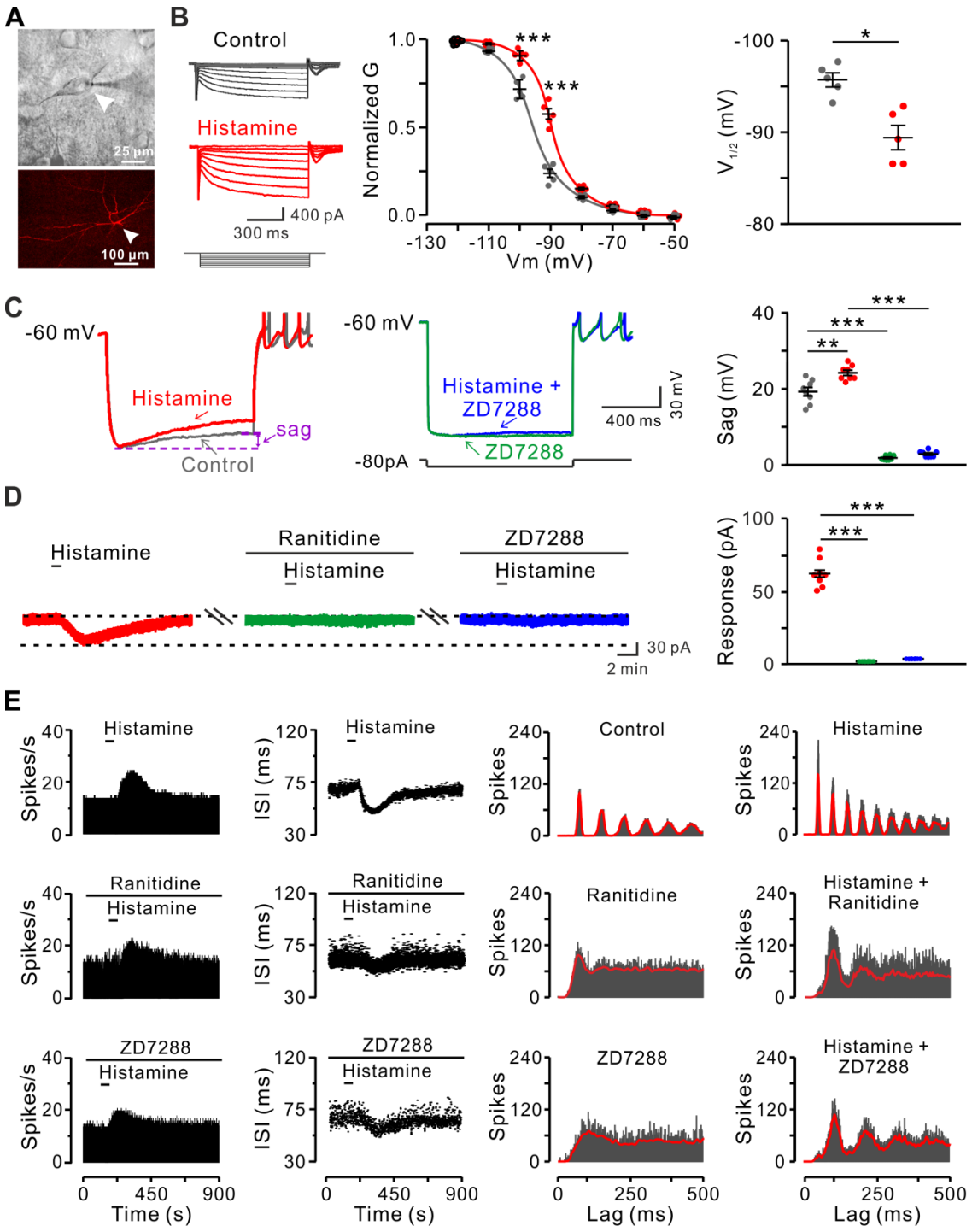
A
25 μm
100 μm
B
Control
Histamine
400 pA
300 ms
Normalized G
1.0
0.5
0.0
***
***
-130 -110 -90 -70 -50
Vm (mV)
-100
-90
-80
V1/2 (mV)
*
C
-60 mV
Histamine
sag
Control
-60 mV
Histamine +
ZD7288
400 ms
30 mV
ZD7288
-80pA
40
20
0
Sag (mV)
***
***
**
D
Histamine
Ranitidine
Histamine
ZD7288
Histamine
30 pA
2 min
100
50
0
Response (pA)
***
***
E
Histamine
Spikes/s
ISI (ms)
Control
Spikes
Ranitidine
Histamine
Histamine +
Ranitidine
ZD7288
Histamine +
ZD7288
0 450 900
Time (s)
0 250 500
Lag (ms)
F
Counts/bin
0 100 200
ISI (ms)
G
CV
0.3
0.15
0
***
Saline
Histamine
Ranitidine
Histamine + Ranitidine
ZD7288
Histamine + ZD7288

Figure 3. HCN channel coupled to H2 receptor mediates the effect of histamine on STN neurons in normal rats. (**A**) Microscope image of a STN neuron (indicated by arrowheads) recorded in a brain slice and labeled with biocytin after patch-clamp recording. (**B**) Histamine (10 μM) shifted the conductance-voltage curve of recorded STN neurons (at -90 mV and -100 mV, *n* = 5). The conductance curve was converted from the whole-cell currents recorded from -50 to -120 mV and was fitted by Boltzmann function. Note that the conductance exhibited a significant feature of hyperpolarization activation and histamine reduced the voltage required for half-maximal activation ($V_{1/2}$, *n* = 5). (**C**) Histamine increased the inward rectification (sag) in response to an 80 pA hyperpolarizing current pulse. ZD7288 (50 μM), a selective blocker for HCN channel, abolished the depolarizing sag in both the absence and presence of histamine (*n* = 8). (**D**) Histamine elicited an inward current in a STN neuron, and ranitidine (1 μM), a selective antagonist for H2 receptor, or ZD7288 (50 μM) totally blocked the current induced by histamine (*n* = 8). (**E** and **F**) PSTHs, scatter plots of ISI series, autocorrelation histograms and an ISI histogram of discharges of a recorded STN neuron show the histamine-induced changes in firing rate and firing pattern in the absence and presence of ranitidine and ZD7288 (1 μM, respectively). (**G**) Group data show that histamine significantly decreased the CV of ISIs, whereas ZD7288 remarkably increased the CV and blocked the histamine-induced decrease in CV (*n* = 30). Data are represented as mean ± SEM; * $P < 0.05$, ** $P < 0.01$, *** $P < 0.001$ by two-tailed paired t-test (**B**) or one-way ANOVA with Newman-Keuls post hoc test (**C**, **D**, and **G**).

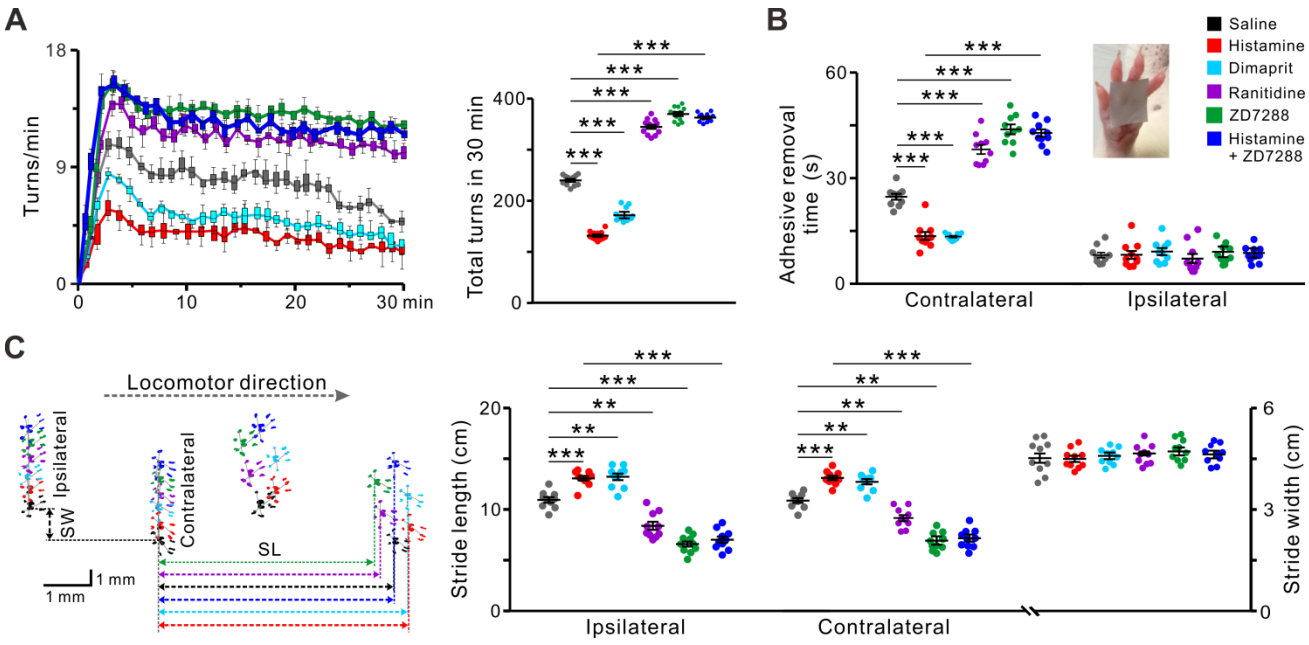

Figure 4. HCN channel coupled to H2 receptor mediates the histamine-induced amelioration of motor deficits in PD rats. Effects of microinjection of histamine (1 μg), dimaprit (a selective agonist for H2 receptor, 2 μg), ranitidine (a selective antagonist for H2 receptor, 3.5 μg), and ZD7288 (a selective blocker for HCN channel, 3 μg) into the STN on turning behavior (**A**, n = 12), adhesive removal test (**B**, n = 10) and locomotor footprints (**C**, n = 10) in PD rats. Dimaprit mimicked the histamine-induced decrease in turnings, shortened time for removing an adhesive strip from forelimb contralateral to the lesion, and enlarged bilateral stride lengths, whereas ranitidine and ZD7288 significantly increased the turnings, prolonged contralesional adhesive removal time, and shortened bilateral stride lengths. ZD7288 also abolished the histamine-induced amelioration of turning, adhesive removal and locomotor behaviors in PD rats. Data are represented as median (horizontal bar) with 25th-75th (box) and 5th-95th (whiskers) percentiles or mean ± SEM; ** P < 0.01, *** P < 0.001 by one-way (**A** and **C**, stride width) or two-way ANOVA (**B** and **C**, stride length) with Newman-Keuls post hoc test.

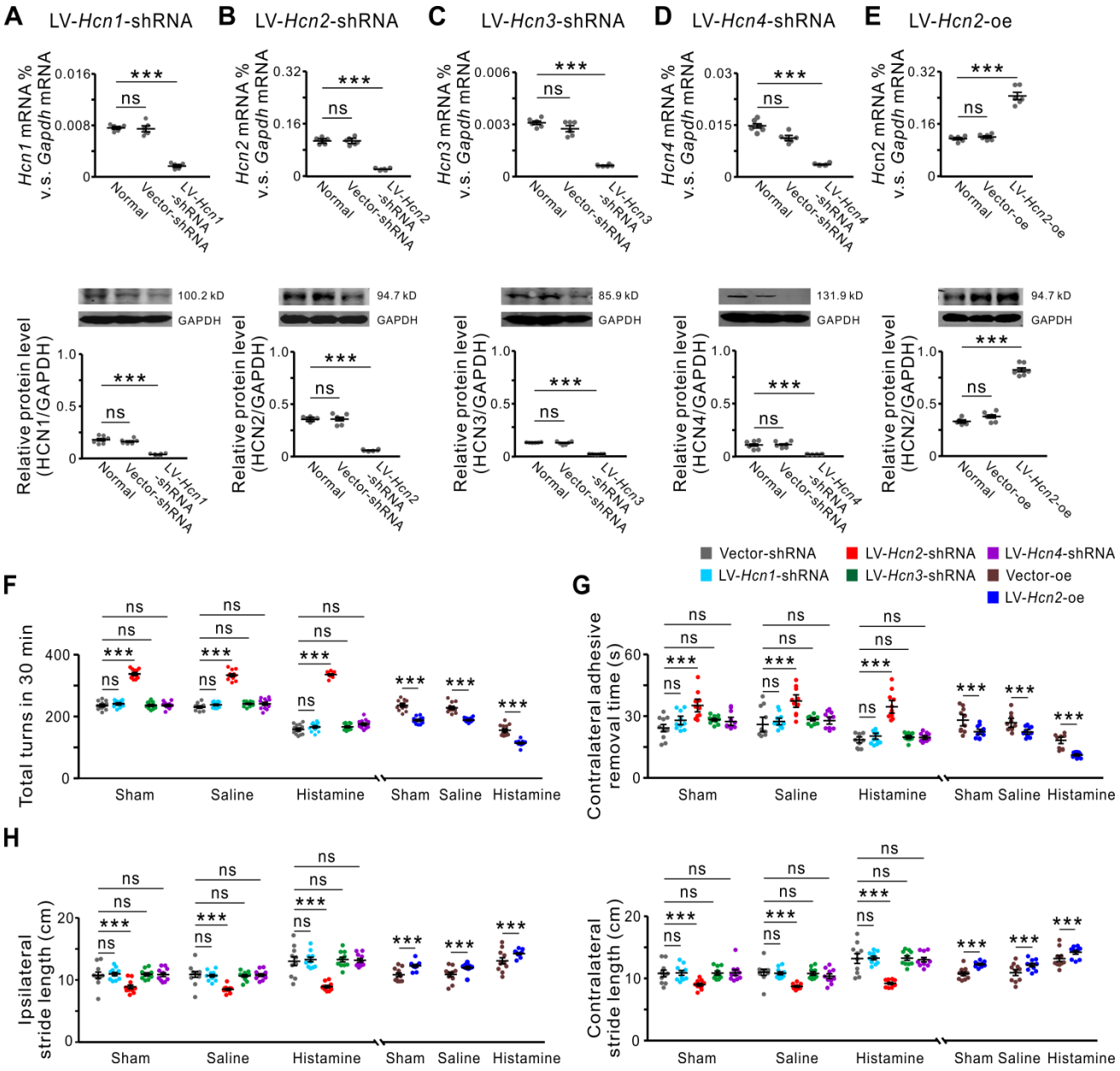

Figure 5. HCN2 channel is responsible for the histamine-induced amelioration of motor deficits in PD rats. (**A-D**) LV-*Hcn1*-shRNA, LV-*Hcn2*-shRNA, LV-*Hcn3*-shRNA and LV-*Hcn4*-shRNA effectively downregulated the expression of *Hcn1, Hcn2, Hcn3 and Hcn4* mRNAs and proteins (*n* = 6 from 6 independent experiments) in the STN. (**E**) LV-*Hcn2*-oe upregulated the expression of *Hcn2* mRNAs and proteins (*n* = 6 from 6 independent experiments). (**F-H**) Effects of downregulation and overexpression of HCN2 channel in the STN on motor deficits of turning behavior (**F,** *n* = 12),

adhesive removal test (**G,** n = 10) and locomotor footprints (**H,** n = 10) in PD rats with sham operation, saline injection and histamine injection. Downregulation of HCN2 channel significantly increased the apomorphine-induced turnings, prolonged contralesional adhesive removal time and shortened bilateral stride length, whereas downregulation of HCN1, HCN3, or HCN4 channel had no effect on these motor deficits. Only the downregulation of HCN2 rather than HCN1, HCN3, or HCN4 channel blocked the amelioration of turnings, removal time and stride length of PD rats induced by microinjection of histamine into the STN. Overexpression of HCN2 channel in STN not only decreased the turnings, reduced removal time and enlarged bilateral stride length of PD rats, but also improved the histamine-induced amelioration in these motor behaviors. Data are represented as mean ± SEM; ns, no statistical difference and *** $P < 0.001$ by one-way (**A-E**) or two-way ANOVA (**F-H**) with Newman-Keuls post hoc test.

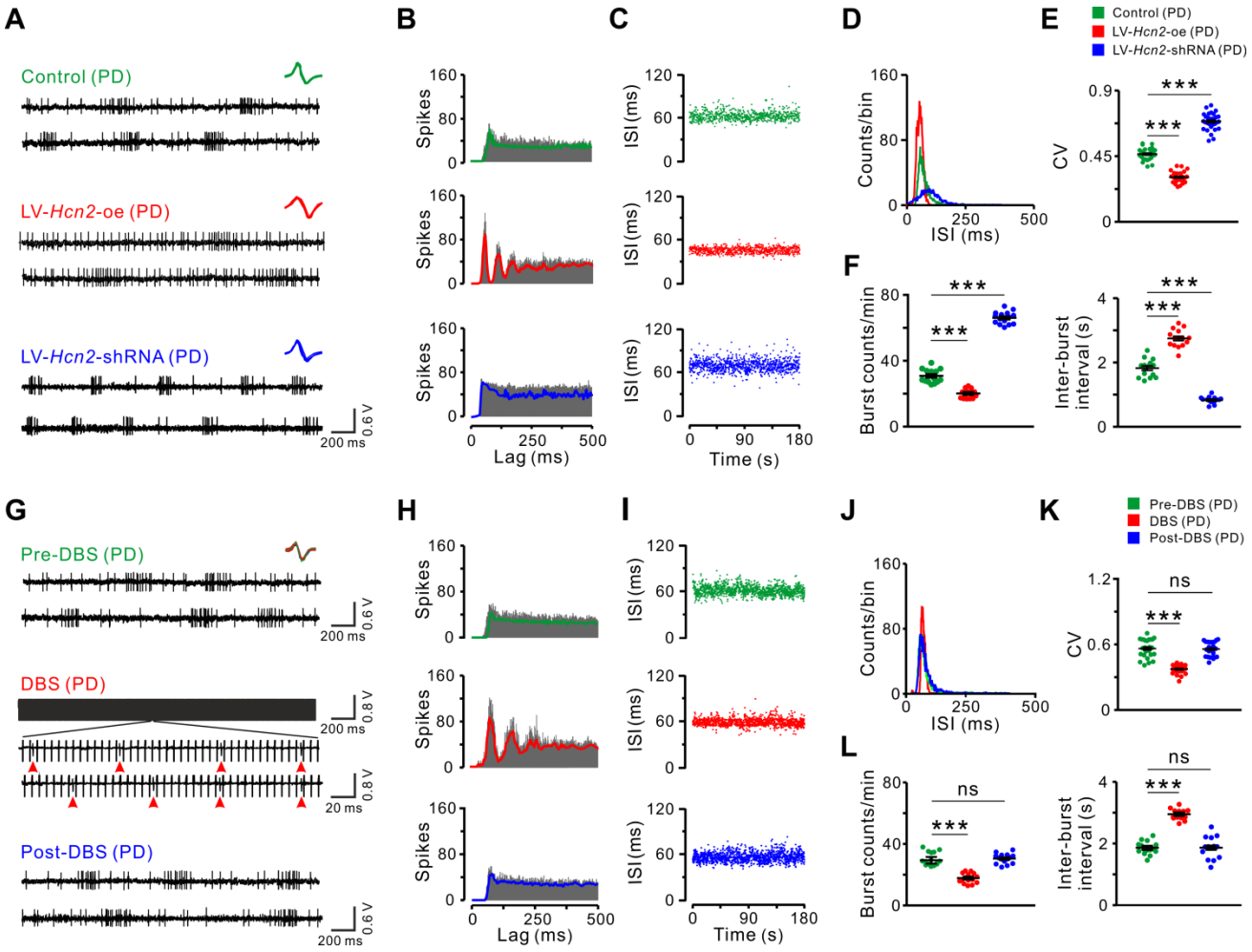

Figure 6. Overexpression of HCN2 channel, as well as STN-DBS, regularizes firing patterns of STN neurons in PD rats. (**A**) Three continuous oscilloscope traces show the firings of three STN neurons in a PD rat, a PD rat with overexpression of HCN2 in STN and a PD rat with downregulation of HCN2, respectively. The insets represent five superimposed traces of spike waveforms for each unit, respectively. (**B-D**) Autocorrelation histograms, scatter plots of ISI series and ISI histograms of three STN neurons presented in (**A**). (**E** and **F**) Overexpression of HCN2 in the STN decreased the CV of ISIs and the number of bursts and increased inter-burst intervals of STN neurons, whereas downregulation of HCN2 increased their CV of ISIs and the number of bursts and decreased inter-burst intervals (**E**, n = 30; **F**, n = 15). (**G**) Three continuous oscilloscope traces show

the firings of a STN neuron in a PD rat before, during and after a high frequency stimulation (125 Hz, 70 μA, 80-μs pulse width), respectively. The red arrows in the zoomed in portion of the spike train during DBS indicate firing spikes of the recorded STN neuron. The insets represent fifteen superimposed traces of spike waveforms for the unit, i.e., 5 traces before (*green*), 5 traces during (*red*), and 5 traces after (*blue*) the stimulation. (**H-J**) Autocorrelation histograms, scatter plots of ISI series and ISI histograms of the STN neuron presented in (**G**). (**K** and **L**) DBS decreased the CV of ISIs (n = 25) and the number of bursts and increased inter-burst intervals of STN neurons (n = 15), indicating DBS regularizes the firing pattern of STN neurons. Data are represented as mean ± SEM; ns, no statistical difference, *** $P < 0.001$ by one-way ANOVA with Newman-Keuls post hoc test (**E**, **F**, **K** and **L**).

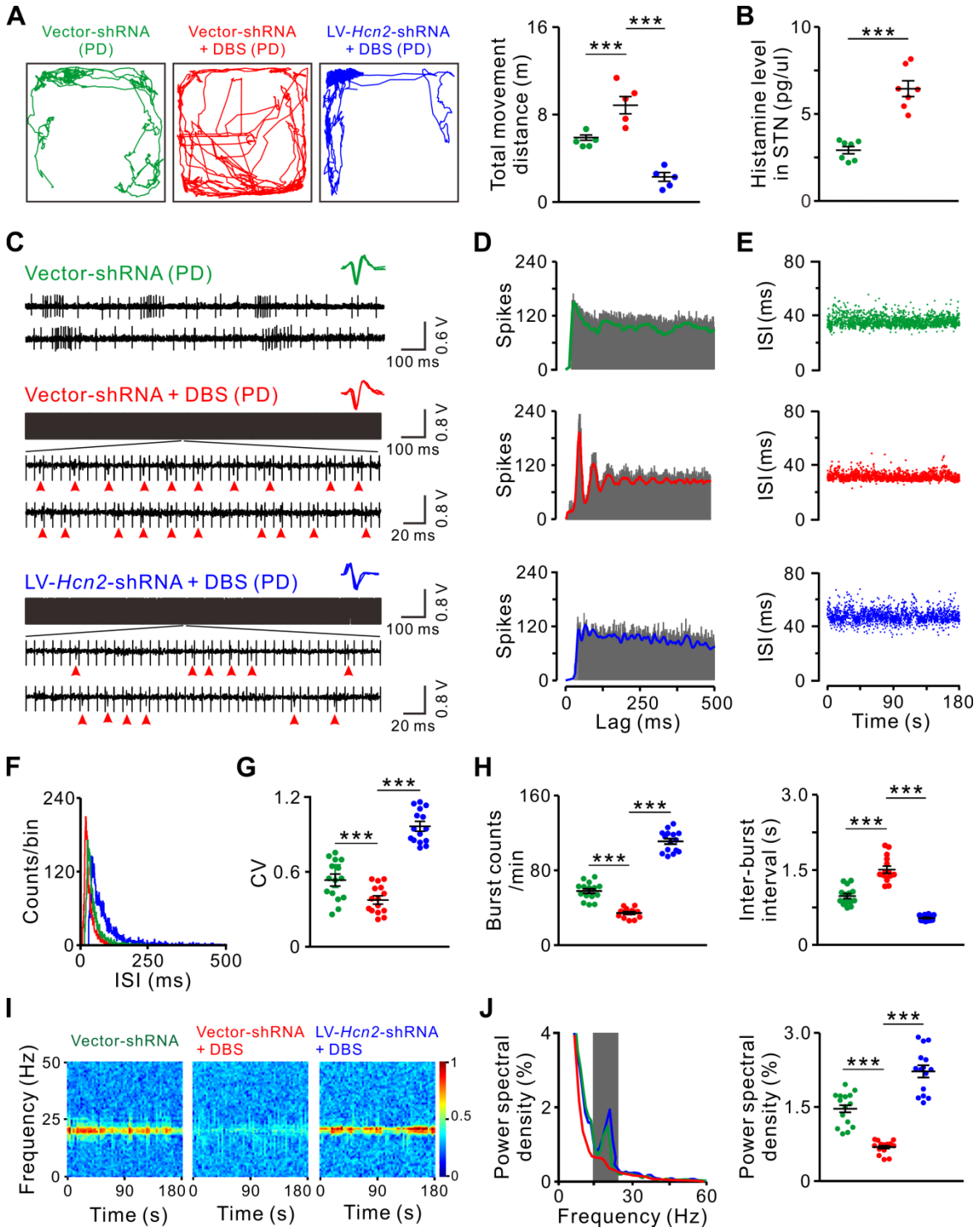

Figure 7. Downregulation of HCN2 attenuates the STN-DBS-induced amelioration of motor dysfunction, firing patterns, and beta oscillations in free-moving PD rats. (**A**) Locomotor traces of PD rats in an open field. STN-DBS increased total movement distance of PD rats, whereas downregulation of HCN2 in STN abolished the DBS-induced motor amelioration (n = 5). (**B**)

STN-DBS increased the histamine release in STN of PD rats in the open field (n = 7). (**C**) Three continuous oscilloscope traces show the firings of three STN neurons in free-moving PD rats treated with control virus, control virus + STN-DBS, or downregulation of HCN2 virus + STN-DBS, respectively. The red arrows indicate firing spikes of the recorded STN neurons during DBS. The insets represent five superimposed traces of spike waveforms for each unit, respectively. (**D-F**) Autocorrelation histograms, scatter plots of ISI series and ISI histograms of three STN neurons presented in (**C**). (**G** and **H**) STN-DBS decreased the CV of ISIs and the number of bursts, and increased inter-burst intervals of STN neurons in free-moving PD rats, whereas downregulation of HCN2 blocked the STN-DBS-induced regularization of neuronal firing patterns (n = 15). (**I**) Power spectrograms of simultaneously recorded local field potentials in STN of these free-moving PD rats in the open field. (**J**) Power spectral distribution of local field potentials recorded from STN. The gray box indicates the classic beta band (15-25 Hz). A clear increase of power in the beta band was found in the PD rats. STN-DBS significantly alleviated the dominant beta band oscillatory activities in PD rats, whereas downregulation of HCN2 abolished the STN-DBS-induced suppression of excessive beta oscillations (n = 15). Data are represented as mean ± SEM; *** $P < 0.001$ by one-way ANOVA with Newman-Keuls post hoc test (**A**, **G**, **H**, and **J**) and two-tailed paired t-test (**B**).